Supplementary Information for

Size-resolved isotope analysis reveals anthropogenic reactive nitrogen transport and transformation in Taiwan mountain forests

Wen-Chien Lee,[1] Ming-Hao Huang,[1] Wei-Chieh Huang,[1] Jen-Ping Chen,[1] Yen-Jen Lai,[2,3] Haojia Ren,[4]* and Hui-Ming Hung[1]*

[1] Department of Atmospheric Sciences, National Taiwan University, Taipei, 10617, Taiwan

[2] Experimental Forest, National Taiwan University, Nantou, 557004, Taiwan

[3] Department of Agricultural Chemistry, National Taiwan University, Taipei, 10617, Taiwan

[4] Department of Geosciences, National Taiwan University, Taipei, 10617, Taiwan

Correspondence to: Haojia Ren (abbyren@ntu.edu.tw) and Hui-Ming Hung (hmhung@ntu.edu.tw)

This PDF file includes:

Number of pages: 21

Number of Descriptions: 3

Number of tables: 1

Number of figures: 15

Description S1. Particle concentration estimated by FTIR analysis

The mass concentration of aerosol particles on the filter samples was estimated using FTIR absorbance spectra. First, specific peaks in the absorbance spectra were identified and quantified, including the NH_4^+ peak at 1417 cm^{-1} in the region of 1405−1450 cm^{-1}, the NO_3^- peak at 1340−1355 cm^{-1}, the SO_4^{2-} peak at 1085 cm^{-1}, and the BC peak at 3945−3955 cm^{-1}. The peaks were fitted with Lorentzian functions to derive the absorbance (*Abs*) of each functional group. FTIR absorbance and mass concentration measured by ion chromatography (IC) were then applied to derive the mass concentrations of the functional groups by assuming a well-distributed sample on the filter:

$$\frac{A_{\mathrm{FTIR}}}{A_{\mathrm{sample}}} \times m \times F \times t_s = \alpha \times Abs \tag{S1}$$

where A_{FTIR} is the FTIR scanning area, A_{sample} is the sampling area on the filter, m is the mass concentration measured by IC, F is the sampling flow rate, t_s is the sampling time, and α is obtained through an experimental regression of IC and FTIR measurements.

Description S2. Calculation of mass-weighted particle diameter (D_{m})

Aerosol particle diameter was determined from filter samples collected using a micro-orifice uniform deposit impactor (MOUDI). To ensure sufficient particle concentrations for isotope analysis, some filter samples were combined. For these combined samples, the particle diameters were calculated as mass-weighted diameters for specific chemical species according to:

$$\log D_{\mathrm{m}} = \frac{\sum_{i=1}^{n}\left(\log D_i \times m_{D_i}\right)}{\sum_{i=1}^{n} m_{D_i}} \tag{S2}$$

where D_{m} is the mass-weighted diameter, D_i is the geometric mean diameter of particles collected in the i^{th} stage of the MOUDI sampler, m_{D_i} is the mass concentration of particles with a diameter D_i determined by FTIR analysis, and n is the number of combined filter samples. Mass-weighted particle diameters were calculated separately for $p\mathrm{NH_4^+}$ and $p\mathrm{NO_3^-}$.

Description S3. Calculation of concentration-weighted $\delta^{15}N\text{-}NH_4^+$, $\delta^{15}N\text{-}NO_3^-$, and $\delta^{18}O\text{-}NO_3^-$

The concentration-weighted means of $\delta^{15}N\text{-}NH_4^+$, $\delta^{15}N\text{-}NO_3^-$, and $\delta^{18}O\text{-}NO_3^-$ were calculated for each sampling period to characterize the isotopic composition. The concentration-weighted mean of a given isotope was determined using the following equation:

$$\delta_{\text{avg}}^{\text{isotope}} = \frac{\sum_{j=1}^{p}\left(\left[X\right]_j \times \delta_j^{\text{isotope}}\right)}{\sum_{j=1}^{p}\left[X\right]_j} \tag{S3}$$

where $\delta_{\text{avg}}^{\text{isotope}}$ is the average isotope value, $[X]_j$ is the mass concentration of compound X in the j^{th} sample, $\delta_j^{\text{isotope}}$ is the isotope value of the j^{th} sample, and p is the total number of samples in the same sampling period. The mass concentrations of pNH_4^+ and pNO_3^- were measured using a fluorometric and a $NO/NO_2/NO_x$ analyzer (Model T200P, Teledyne API), respectively.

Table S1. Ranges of $\delta^{15}N\text{-}NH_3$ values (mean±SD‰) from fertilizer, waste, NH_3 slip, and fossil fuel (Kawashima et al., 2023).

Source types	$\delta^{15}N\text{-}NH_3$	Statistic number
Fertilizer	−28.3±5.8	21
Waste	−17.6±5.6	51
NH_3 slip	−8.2±5.5	9
Fossil fuel	1.8±3.2	38

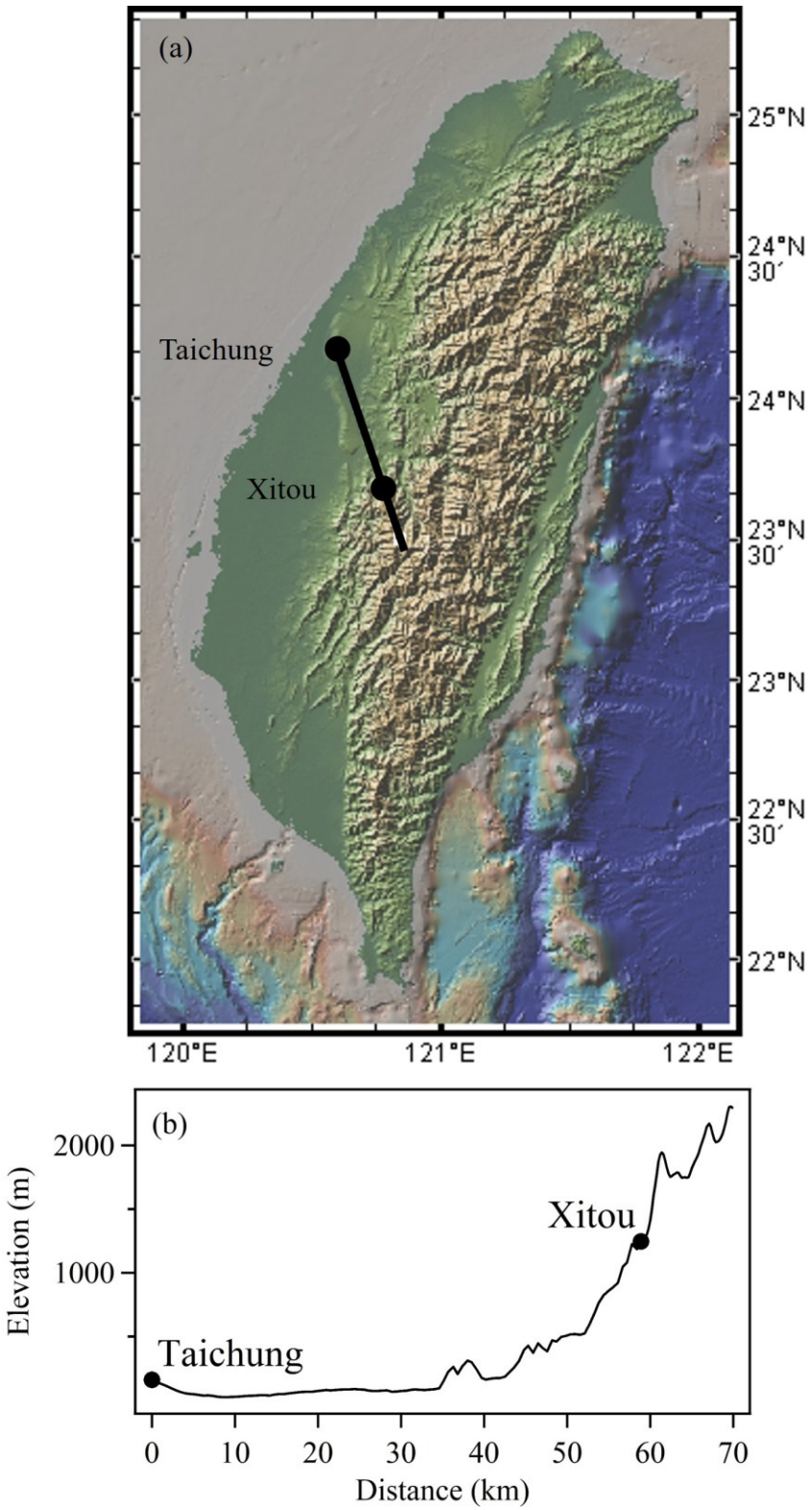

Figure S1. (a) Horizontal distance between the sampling location (Xitou) and Taichung, plotted using GeoMapApp (ver 3.7.4). (b) Elevation profile along the same transect between the sampling location (Xitou) and Taichung.

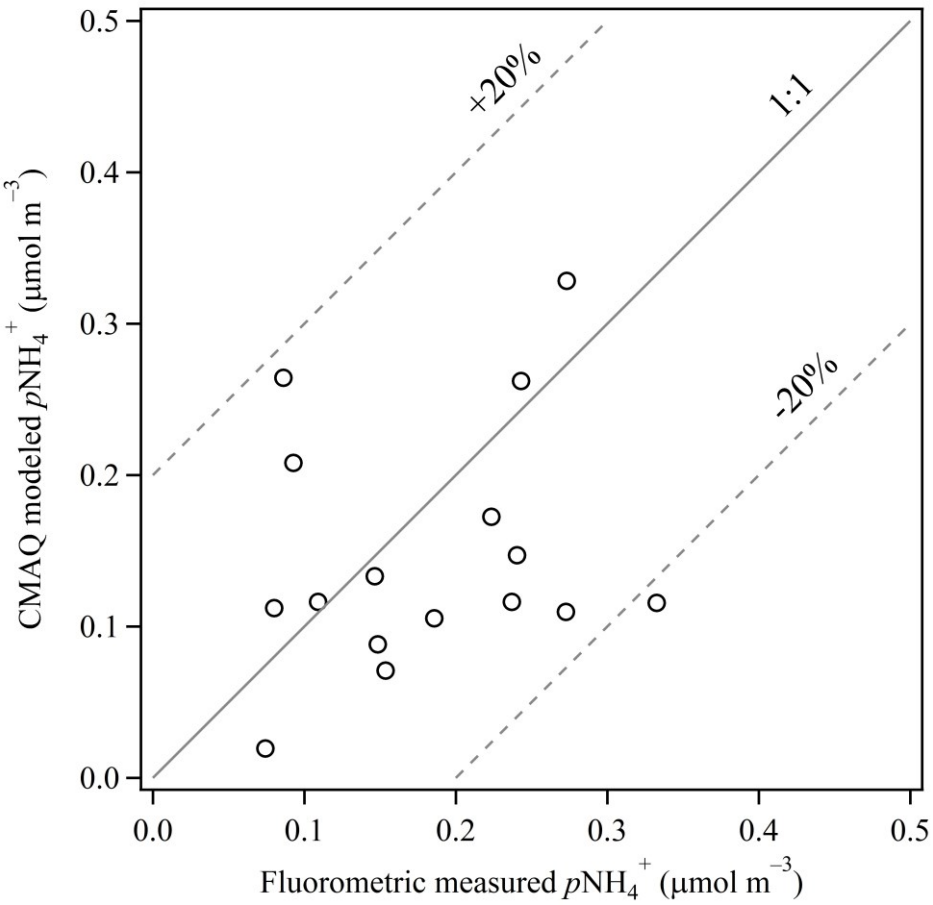

Figure S2. pNH_4^+ concentration measured by fluorometric versus those estimated by CMAQ analysis.

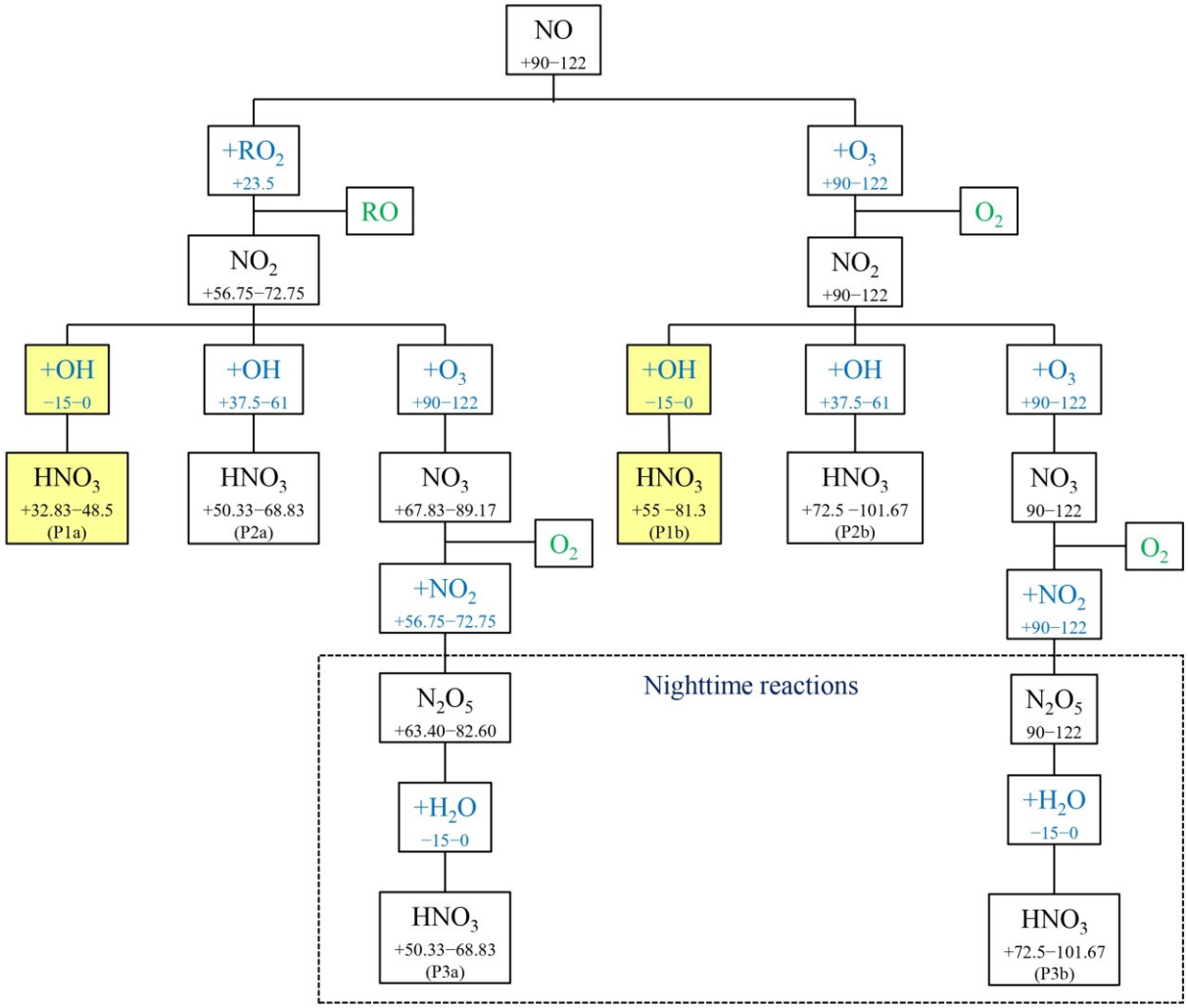

Figure S3. Estimated $\delta^{18}O$ (‰) during HNO_3 formation adapted from Chen et al. (2022). Yellow boxes indicate OH directly derived from the oxygen atom in H_2O.

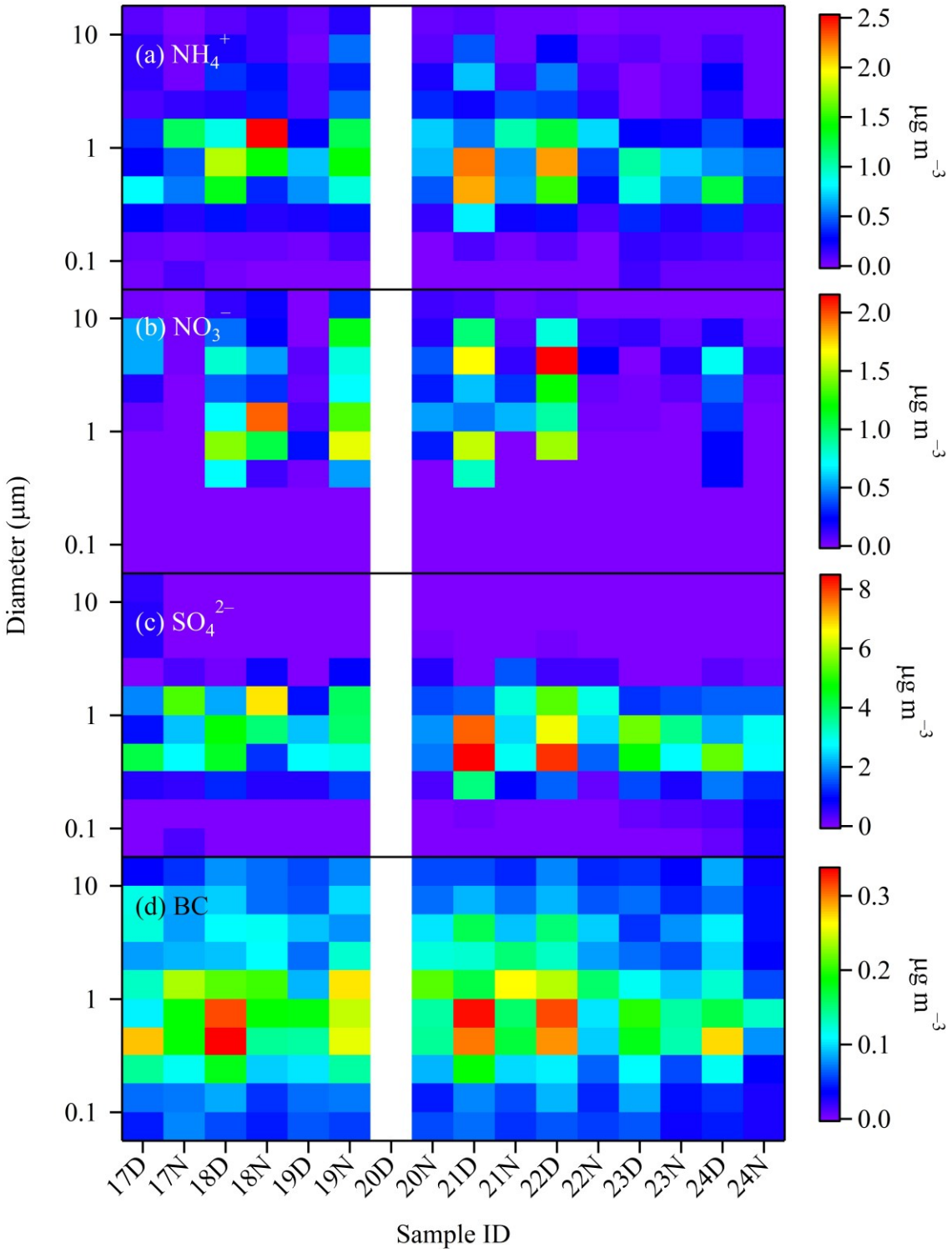

Figure S4. Size-resolved aerosol (a) NH_4^+, (b) NO_3^-, (c)SO_4^{2-}, and (d) BC concentrations.

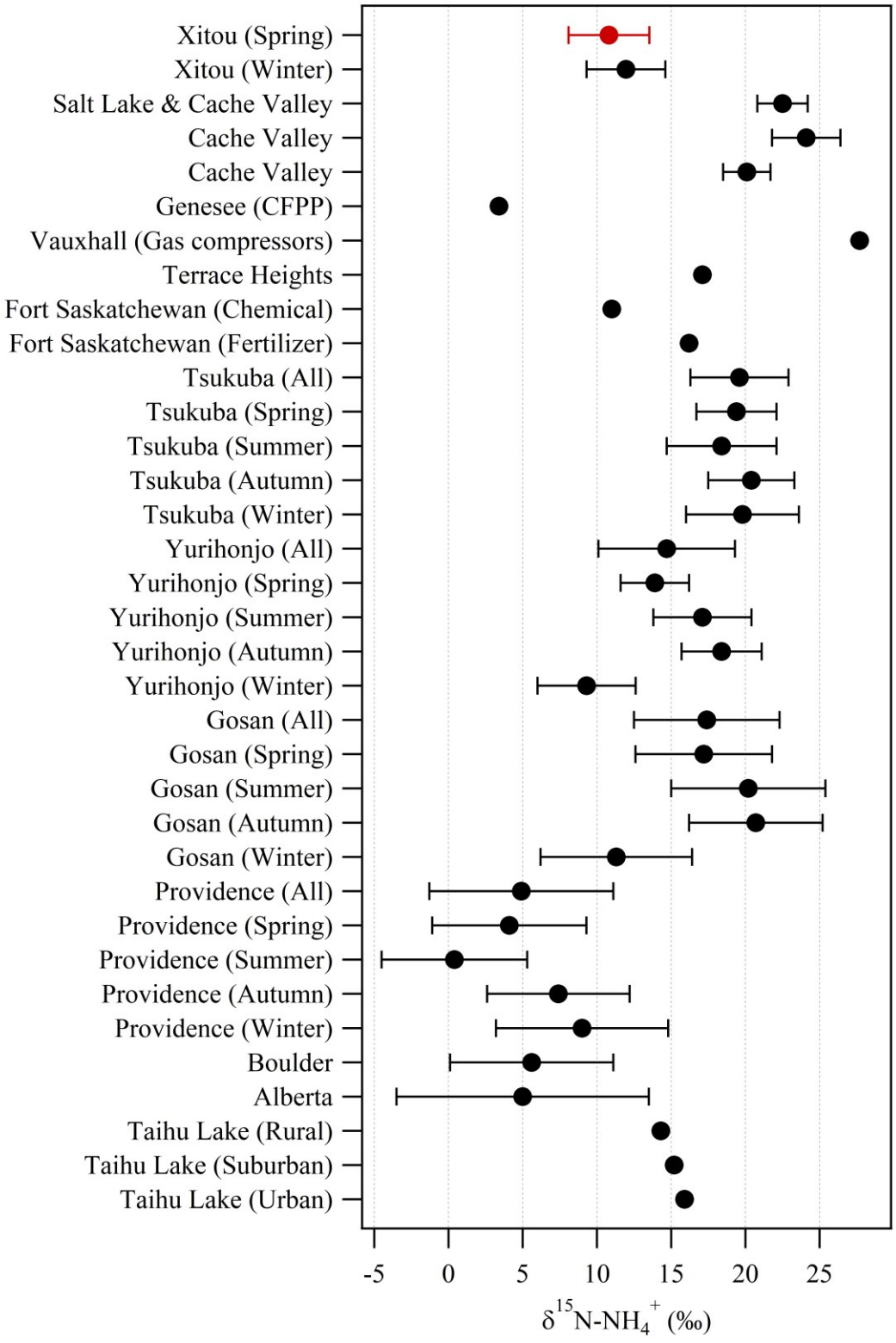

Figure S5. Particulate $\delta^{15}N\text{-}NH_4^+$ measured in this study (red symbol) and reported in the literature (Chen et al., 2022; Savard et al., 2018; Proemse et al., 2012; Hall et al., 2016; Moore, 1977; Kundu et al., 2010; Walters et al., 2022; Kawashima et al., 2023; Ti et al., 2018).

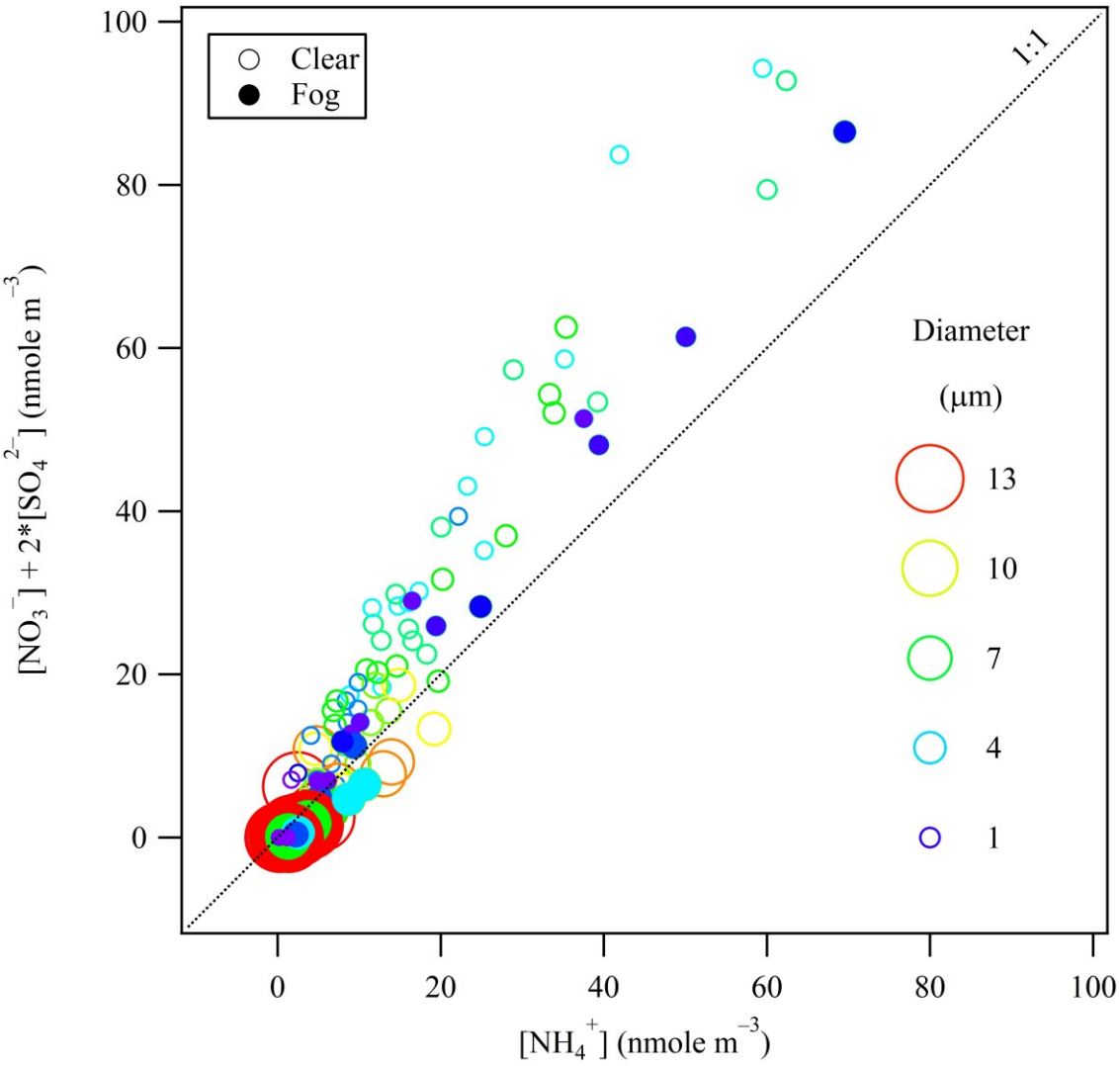

Figure S6. Scatter plot of $[NO_3^-] + 2*[SO_4^{2-}]$ versus $[NH_4^+]$ measured during the observation period.

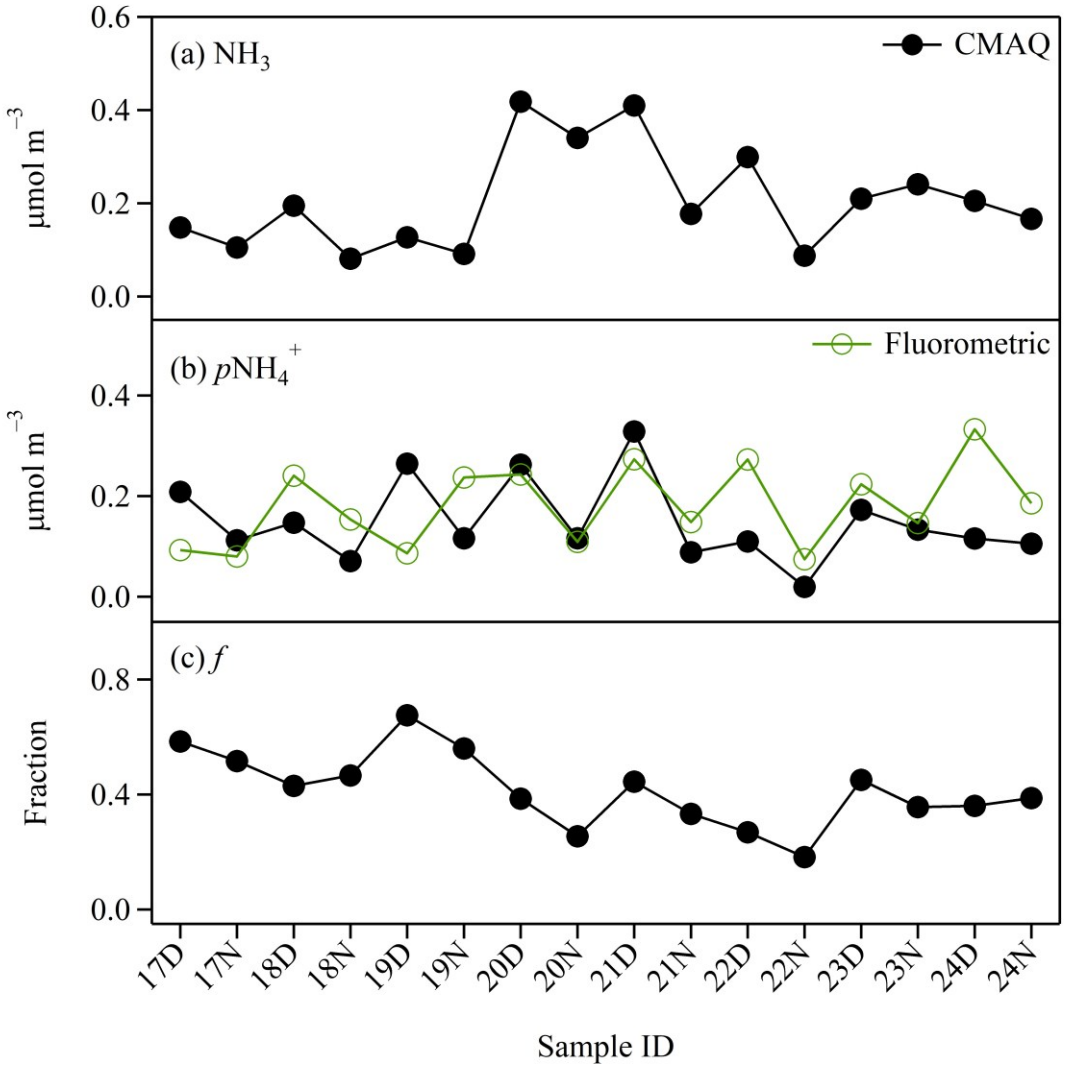

Figure S7. Resulting concentration of (a) NH_3, (b) NH_4^+, and (c) the estimated *f* from fluorometric and CMAQ analysis.

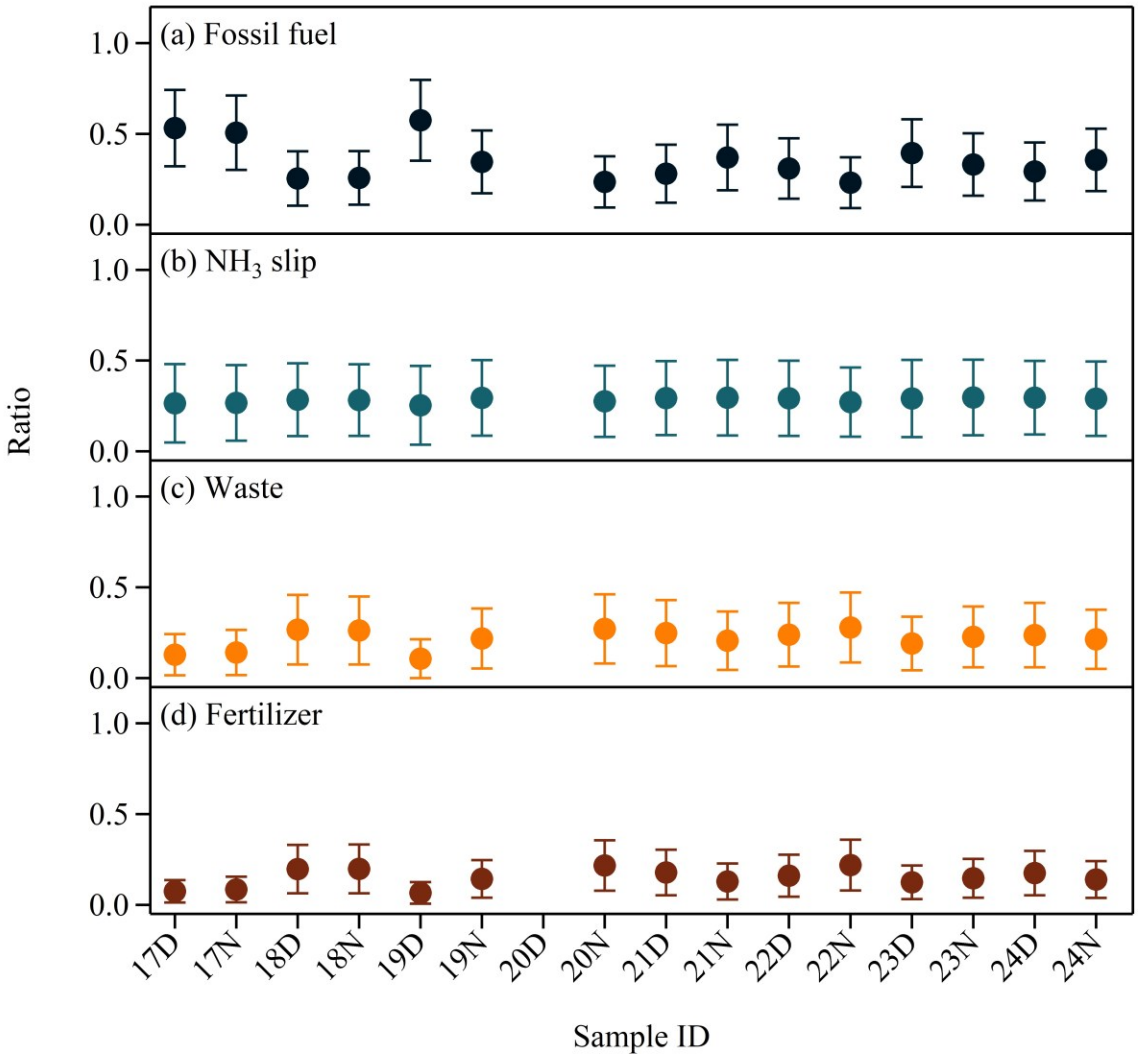

Figure S8. Source apportionment results for NH_3 from the MixSIAR framework for (a) fossil fuel, (b) NH_3 slip, (c) waste, and (d) fertilizer.

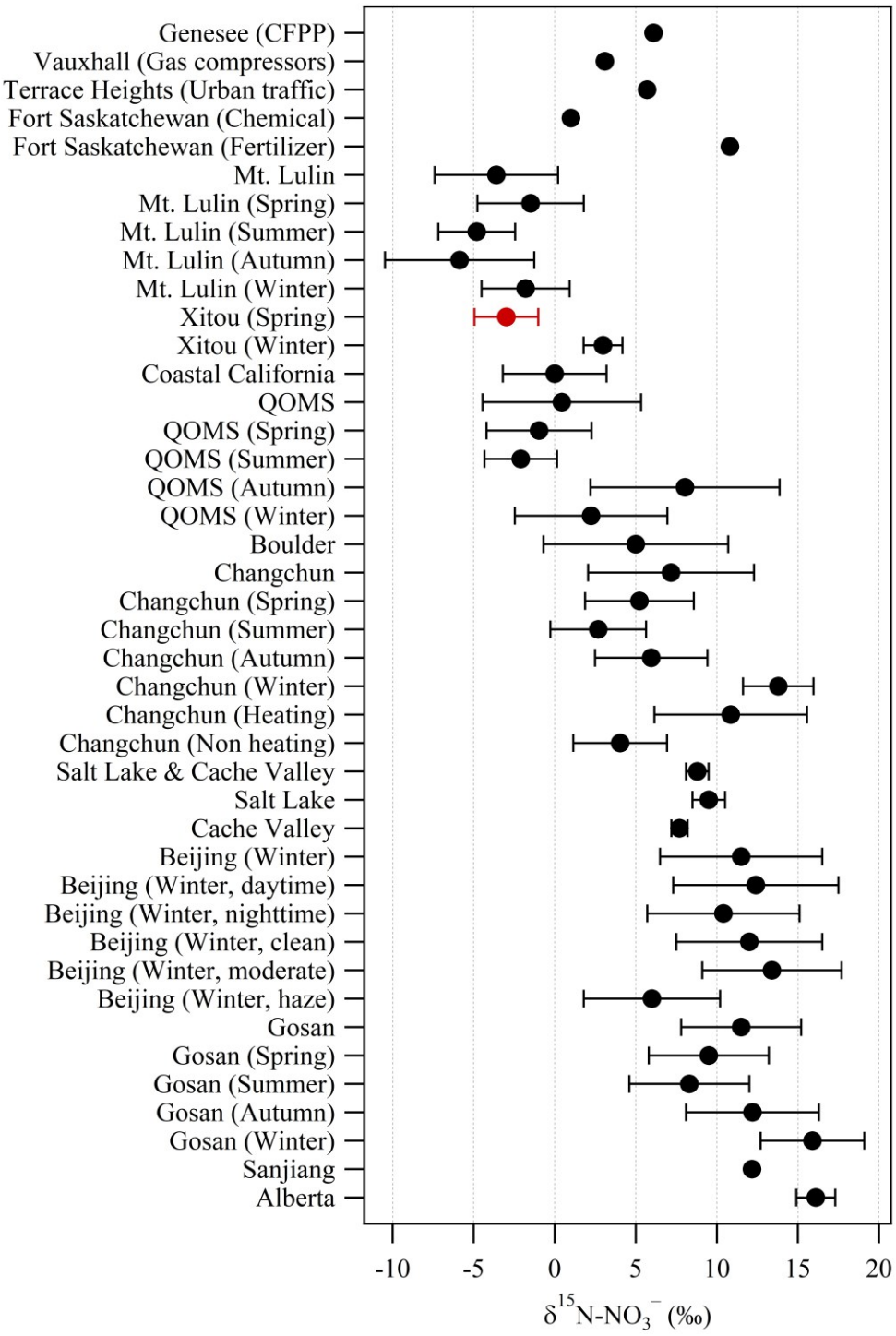

Figure S9. Particulate $\delta^{15}N\text{-}NO_3^-$ measured in this study (red symbol) and reported in the literature (Savard et al., 2018; Guha et al., 2017; Chen et al., 2022; Vicars et al., 2013; Lin et al., 2021; Moore, 1977; Zhao et al., 2020; Hall et al., 2016; Fan et al., 2020; Kundu et al., 2010; Chang et al., 2018; Proemse et al., 2012).

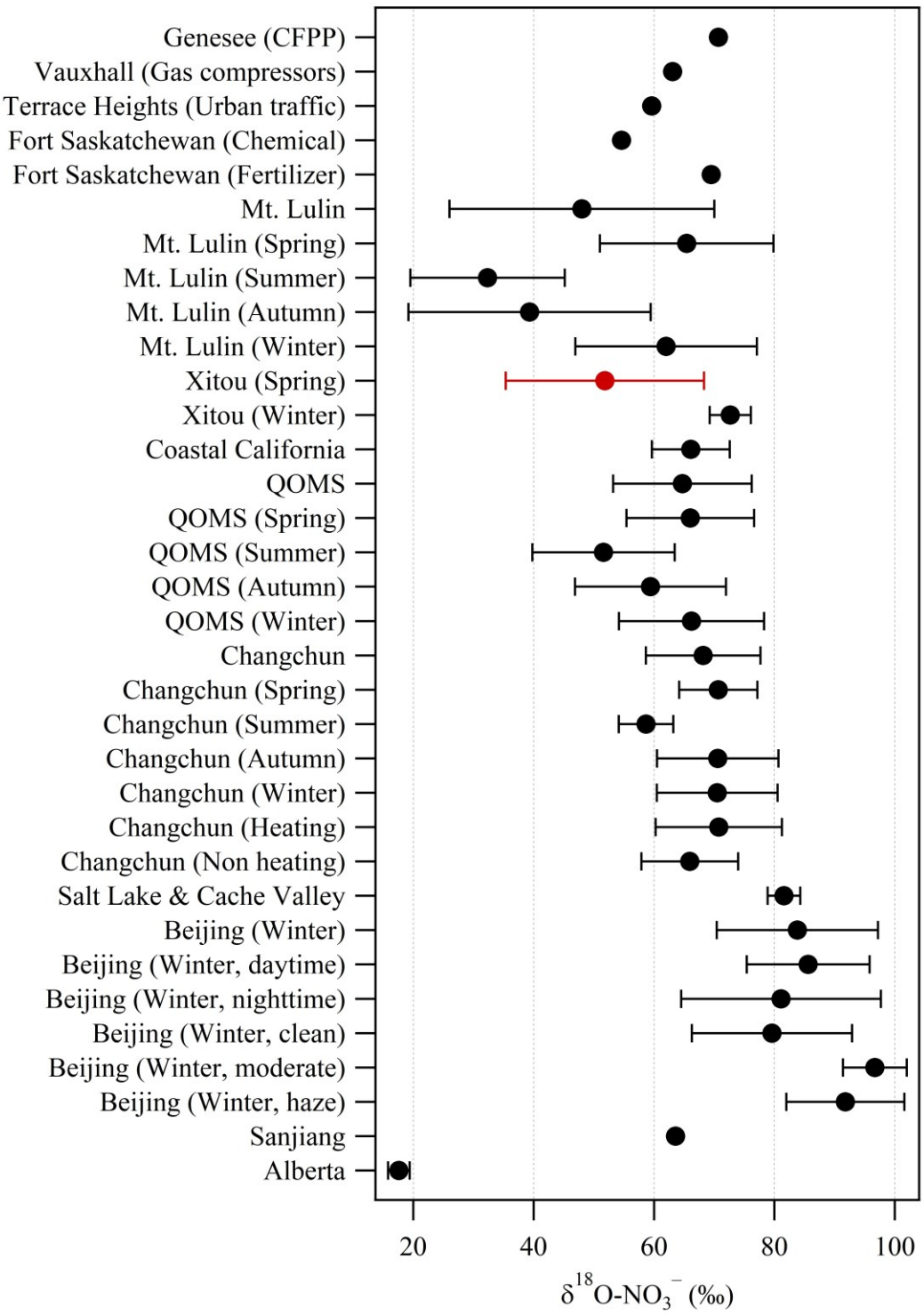

Figure S10. Particulate $\delta^{18}O\text{-}NO_3^-$ measured in this study (red symbol) and reported in the literature (Savard et al., 2018; Guha et al., 2017; Chen et al., 2022; Vicars et al., 2013; Lin et al., 2021; Zhao et al., 2020; Hall et al., 2016; Fan et al., 2020; Chang et al., 2018; Proemse et al., 2012).

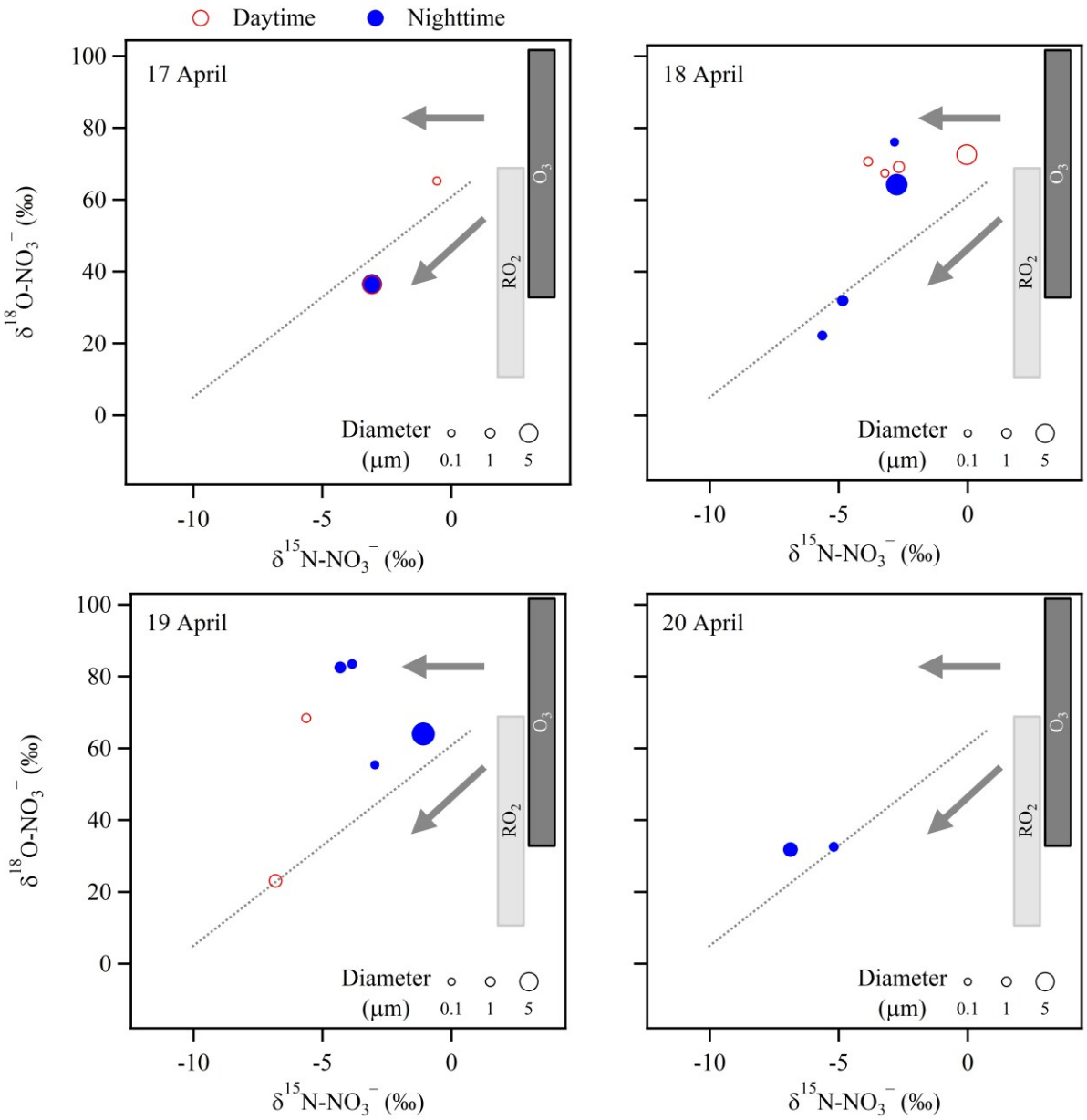

Figure S11. Daily size-resolved isotopic composition of pNO_3^- from 17 to 20 April.

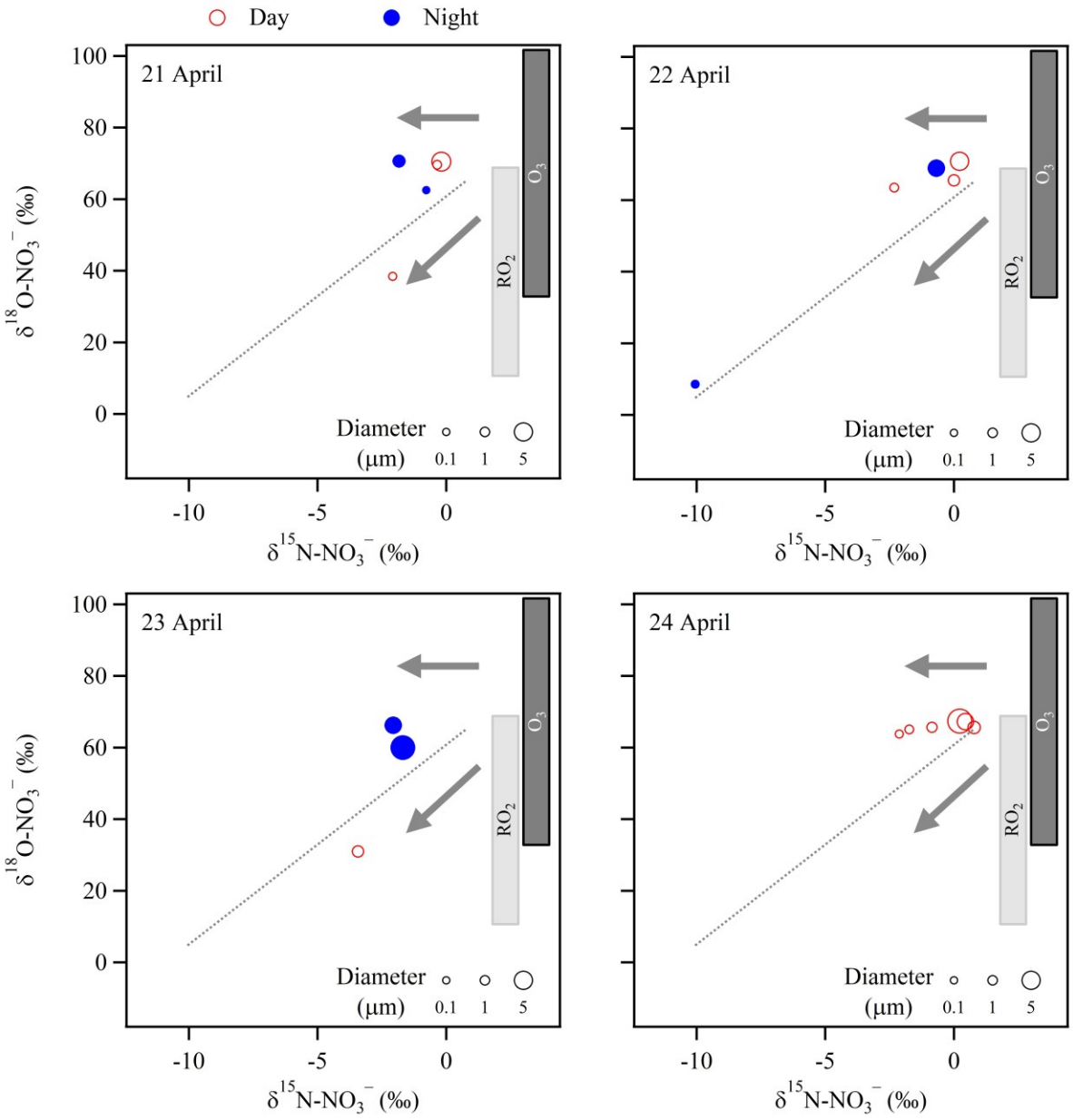

Figure S12. Daily size-resolved isotopic composition of pNO_3^- from 21 to 24 April.

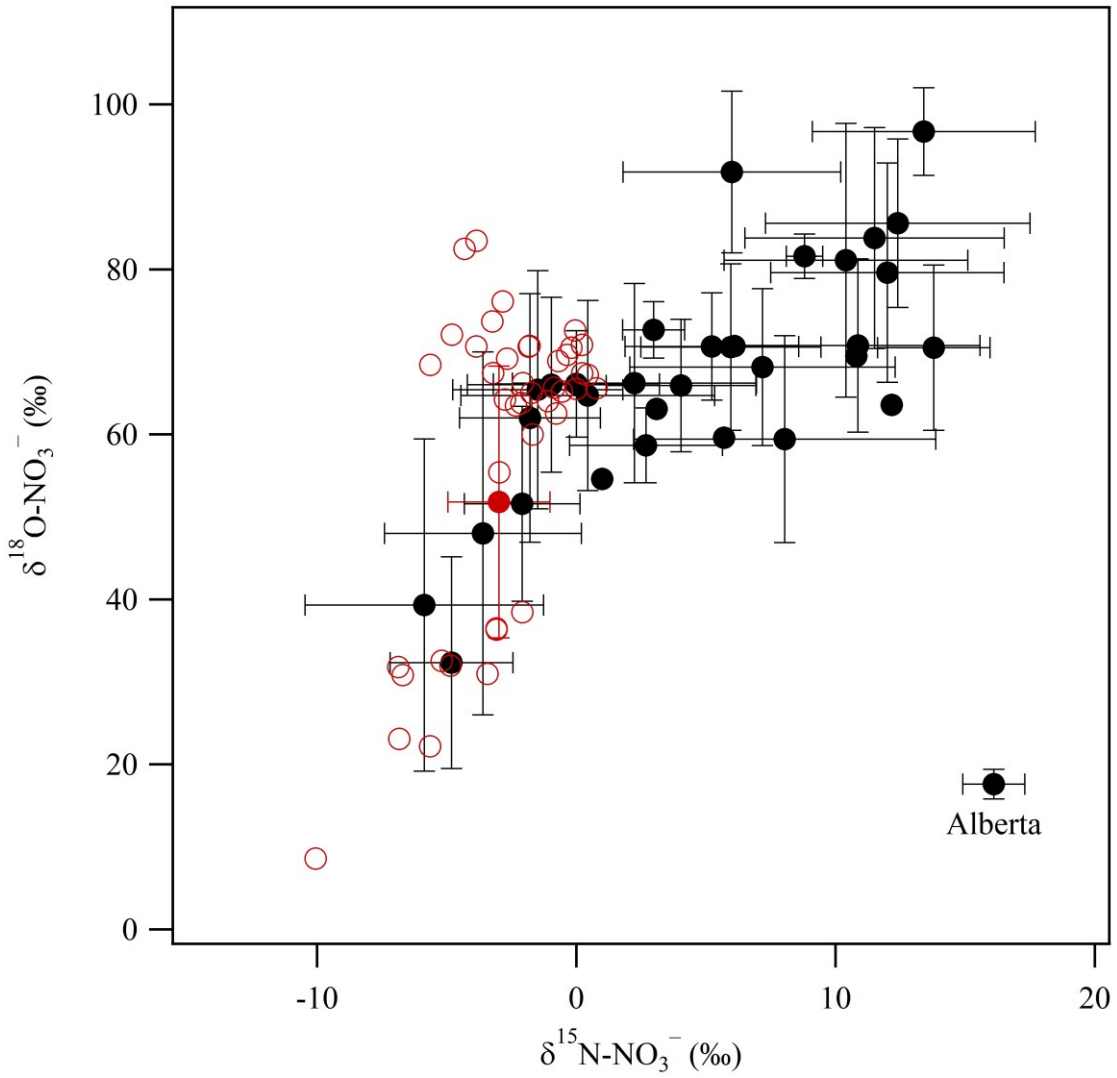

Figure S13. Relationship between particulate $\delta^{15}N\text{-}NO_3^-$ versus $\delta^{18}O\text{-}NO_3^-$ in this study (red symbols) and reported in the literature (Savard et al., 2018; Guha et al., 2017; Chen et al., 2022; Vicars et al., 2013; Lin et al., 2021; Zhao et al., 2020; Hall et al., 2016; Fan et al., 2020; Chang et al., 2018; Proemse et al., 2012). Red open circles represent individual measurements from this study, while the red solid circle denotes the mean value.

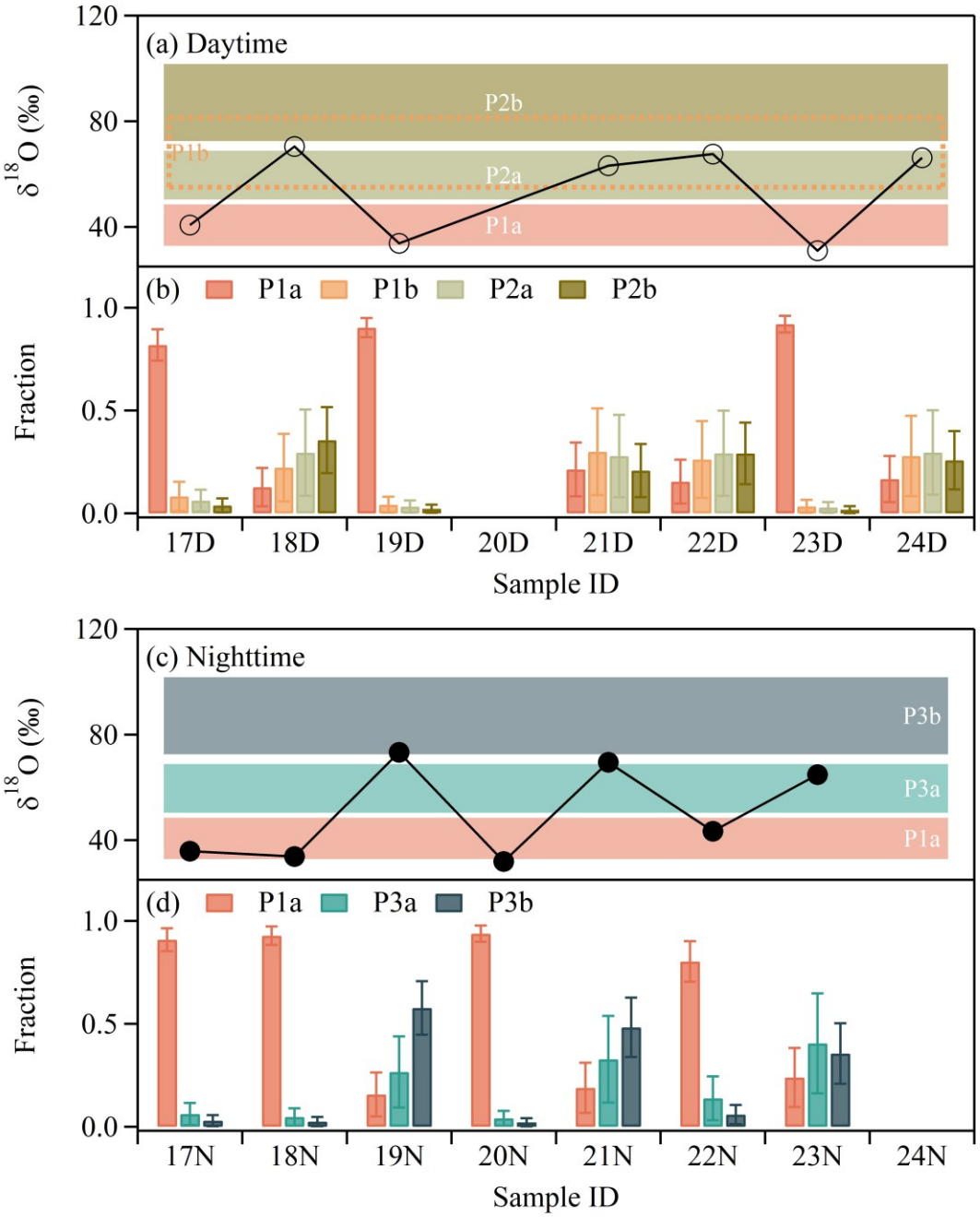

Figure S14. Contributions of nitrate formation pathways estimated by MixSIAR. (a, c) Measured $\delta^{18}O$-NO_3^- values with the corresponding $\delta^{18}O$ ranges of potential formation pathways. (b, d) estimated fractional contributions of these pathways (*c.f.*, Fig. S3).

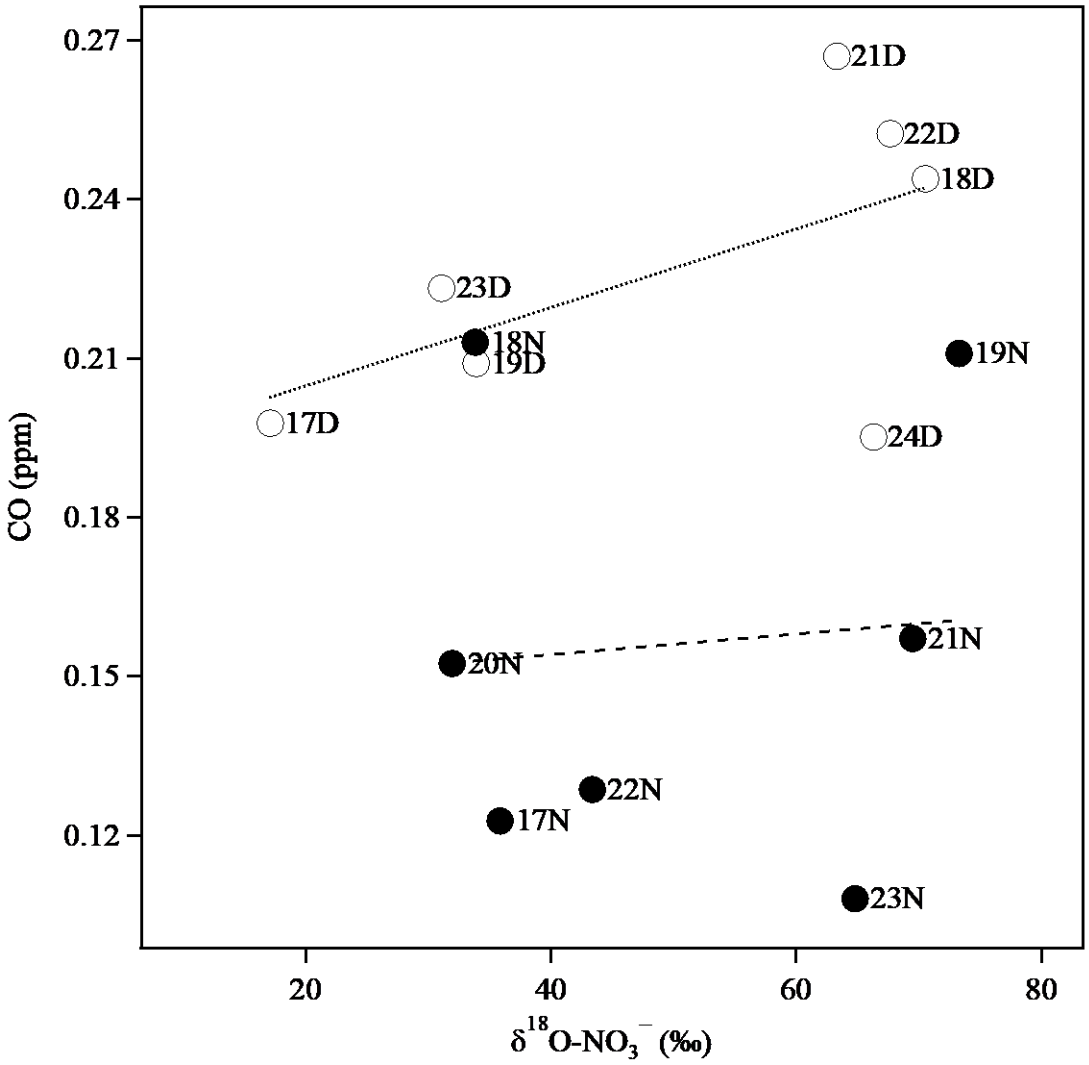

Figure S15. Correlation between daily-averaged CO concentration and $\delta^{18}O\text{-}NO_3^-$.

References

Chang, Y., Zhang, Y., Tian, C., Zhang, S., Ma, X., Cao, F., Liu, X., Zhang, W., Kuhn, T., and Lehmann, M. F.: Nitrogen isotope fractionation during gas-to-particle conversion of NO_x to NO_3^- in the atmosphere – implications for isotope-based NO_x source apportionment, Atmos. Chem. Phys., 18, 11647-11661, https://doi.org/10.5194/acp-18-11647-2018, 2018.

Chen, T. Y., Chen, C. L., Chen, Y. C., Chou, C. C. K., Ren, H., and Hung, H. M.: Source apportionment and evolution of N-containing aerosols at a rural cloud forest in Taiwan by isotope analysis, Atmos. Chem. Phys., 22, 13001-13012, https://doi.org/10.5194/acp-22-13001-2022, 2022.

Fan, M.-Y., Zhang, Y.-L., Lin, Y.-C., Cao, F., Zhao, Z.-Y., Sun, Y., Qiu, Y., Fu, P., and Wang, Y.: Changes of emission sources to nitrate aerosols in Beijing after the clean air actions: Evidence from dual isotope compositions, J. Geophys. Res.: Atmos., 125, e2019JD031998, https://doi.org/10.1029/2019JD031998, 2020.

Guha, T., Lin, C. T., Bhattacharya, S. K., Mahajan, A. S., Ou-Yang, C.-F., Lan, Y.-P., Hsu, S. C., and Liang, M.-C.: Isotopic ratios of nitrate in aerosol samples from Mt. Lulin, a high-altitude station in Central Taiwan, Atmos. Environ., 154, 53-69, https://doi.org/10.1016/j.atmosenv.2017.01.036, 2017.

Hall, S. J., Ogata, E. M., Weintraub, S. R., Baker, M. A., Ehleringer, J. R., Czimczik, C. I., and Bowling, D. R.: Convergence in nitrogen deposition and cryptic isotopic variation across urban and agricultural valleys in northern Utah, J. Geophys. Res.: Biogeosci., 121, 2340-2355, https://doi.org/10.1002/2016JG003354, 2016.

Kawashima, H., Yoshida, O., and Suto, N.: Long-term source apportionment of ammonium in $PM_{2.5}$ at a suburban and a rural site using stable nitrogen isotopes, Environ. Sci. Technol., 57, 1268-1277, https://doi.org/10.1021/acs.est.2c06311, 2023.

Kundu, S., Kawamura, K., and Lee, M.: Seasonal variation of the concentrations of nitrogenous species and their nitrogen isotopic ratios in aerosols at Gosan, Jeju Island: Implications for atmospheric processing and source changes of aerosols, J. Geophys. Res.: Atmos., 115, D20305, https://doi.org/10.1029/2009JD013323, 2010.

Lin, Y.-C., Zhang, Y.-L., Yu, M., Fan, M.-Y., Xie, F., Zhang, W.-Q., Wu, G., Cong, Z., and Michalski, G.: Formation mechanisms and source apportionments of airborne nitrate aerosols at a Himalayan-Tibetan Plateau site: Insights from nitrogen and oxygen isotopic compositions, Environ. Sci. Technol., 55, 12261-12271, https://doi.org/10.1021/acs.est.1c03957, 2021.

Moore, H.: The isotopic composition of ammonia, nitrogen dioxide and nitrate in the atmosphere, Atmos. Environ., 11, 1239-1243, https://doi.org/10.1016/0004-6981(77)90102-0, 1977.

Proemse, B. C., Mayer, B., Chow, J. C., and Watson, J. G.: Isotopic characterization of nitrate, ammonium and sulfate in stack $PM_{2.5}$ emissions in the Athabasca Oil Sands Region, Alberta, Canada, Atmos. Environ., 60, 555-563, https://doi.org/10.1016/j.atmosenv.2012.06.046, 2012.

Savard, M. M., Cole, A. S., Vet, R., and Smirnoff, A.: The $\Delta^{17}O$ and $\delta^{18}O$ values of atmospheric nitrates simultaneously collected downwind of anthropogenic sources – implications for polluted air masses, Atmos. Chem. Phys., 18, 10373-10389, https://doi.org/10.5194/acp-18-10373-2018, 2018.

Ti, C., Gao, B., Luo, Y., Wang, X., Wang, S., and Yan, X.: Isotopic characterization of NH_x-N in deposition and major emission sources, Biogeochemistry, 138, 85-102, https://doi.org/10.1007/s10533-018-0432-3, 2018.

Vicars, W. C., Morin, S., Savarino, J., Wagner, N. L., Erbland, J., Vince, E., Martins, J. M. F., Lerner, B. M., Quinn, P. K., Coffman, D. J., Williams, E. J., and Brown, S. S.: Spatial and diurnal variability in reactive nitrogen oxide chemistry as reflected in the isotopic composition of atmospheric nitrate: Results from the CalNex 2010 field study, J. Geophys. Res.: Atmos., 118, 10,567-510,588, https://doi.org/10.1002/jgrd.50680, 2013.

Walters, W. W., Karod, M., Willcocks, E., Baek, B. H., Blum, D. E., and Hastings, M. G.: Quantifying the importance of vehicle ammonia emissions in an urban area of northeastern USA utilizing nitrogen isotopes, Atmos. Chem. Phys., 22, 13431-13448, https://doi.org/10.5194/acp-22-13431-2022, 2022.

Zhao, Z.-Y., Cao, F., Fan, M.-Y., Zhang, W.-Q., Zhai, X.-Y., Wang, Q., and Zhang, Y.-L.: Coal and biomass burning as major emissions of NO_X in Northeast China: Implication from dual isotopes analysis of fine nitrate aerosols, Atmos. Environ., 242, 117762, https://doi.org/10.1016/j.atmosenv.2020.117762, 2020.